SIMULATION OF HIGH ANGLE-OF-ATTACK FLOW OVER A HEMISPHERE-CYLINDER

Olympio Achilles de Faria Mello - oamello@iae.cta.br
João Luiz Filgueiras de Azevedo - azevedo@iae.cta.br
Instituto de Aeronáutica e Espaço, Centro Técnico Aeroespacial
12228-904 - São José dos Campos - SP, Brazil

Abstract. *A simulation of high angle-of-attack flow over a hemisphere-cylinder body is presented. The Reynolds-averaged Navier-Stokes equations are solved using a diagonal form of an alternating-direction implicit (ADI) approximate factorization procedure. A modified Baldwin-Lomax turbulence model is used. Computed pressure coefficient distributions at angles of attack up to 19 degrees are compared with experimental data. Qualitative evaluation of main flow features, based on local Mach number and skin friction distributions are also analyzed with respect to experimental visualization results. The present work is used to validate the method for simulation of high angle-of-attack flow around sounding rockets and launch vehicles.*

Keywords: *Separated flow, Transonic flow, Computational aerodynamics.*

1. INTRODUCTION

The first attempted launch of the Brazilian Satellite Launch Vehicle (VLS) occurred in November 1997 and was unsuccessful. Flight data indicated that the vehicle attained very high attitudes, outside the expected operational envelope, although this was not a contributing factor to the launch attempt failure. Nevertheless, as part of the post-flight analysis, aerodynamic loads acting on the vehicle were to be estimated for structural analysis purposes. These loads were not available from wind tunnel tests nor from previous computations. A first attempt to estimate these loads was based on a simple interpolation between experimental data available for low angles of attack and take-off configurations. In this initial estimate, the load distribution was assumed to be the same as that for low angles. The shortcomings of these initial estimates are clear: at high angles of attack, flow separation would occur and change the load distribution. Therefore, there was a need for a better estimate of the loads acting on the VLS at high angles. A numerical investigation was then carried out to that effect (Mello & Azevedo, 1999). However, the code used in that work was only partially validated using experimental results obtained at low angles of attack. The investigation presented here was motivated by the need to validate the numerical procedure for use at high angles of attack for future applications to sounding rockets and launch vehicles.

2. NUMERICAL FORMULATION

The numerical procedure used in this work solves the three-dimensional Reynolds-averaged Navier-Stokes (RANS) equations. The solver was adapted from the method developed by Sankar & Kwon (1990). The vector form of the full Reynolds-averaged, 3-D Navier-Stokes equations based on an arbitrary curvilinear coordinate system can be written in non-dimensional form as:

$$\mathbf{Q}_\tau + \mathbf{E}_\xi + \mathbf{F}_\eta + \mathbf{G}_\zeta = \frac{1}{\mathrm{Re}}\left(\mathbf{R}_\xi + \mathbf{S}_\eta + \mathbf{T}_\zeta\right) \tag{1}$$

where **Q** is the vector of unknown flow properties; **E**, **F**, **G** are the inviscid flux vectors; **R**, **S**, **T** are the viscous flux vectors and $\mathrm{Re} = \rho_\infty a_\infty c/\mu_\infty$ is the Reynolds number based on the free-stream speed of sound a_∞, density ρ_∞, viscosity μ_∞ and reference length c.

The time derivative, $\mathbf{Q}_\tau$, of equation (1) is approximated using two-point backward difference at the new time level $n+1$. All spatial derivatives are approximated by standard second-order central differences and are represented by the difference operators δ. The streamwise and normal derivatives, $\mathbf{E}_\xi$ and $\mathbf{G}_\zeta$, are evaluated implicitly at the new time level $n+1$. The azimuthal derivative, $\mathbf{F}_\eta$, is evaluated explicitly at the old time level n but uses the $n+1$ values as soon as they become available. This semi-explicit treatment of the azimuthal derivative enables the scheme to solve implicitly for $\Delta\mathbf{Q}^{n+1}$ at all points at a given azimuthal station at a time. To eliminate any dependency the solution may have on the sweeping direction, the solver reverses the direction of azimuthal sweeping with every sweep.

The viscous terms $\mathbf{R}_\xi$, $\mathbf{S}_\eta$ and $\mathbf{T}_\zeta$ are evaluated explicitly, using half-point central differences denoted here by the difference operator $\overline{\delta}$, so that the computational stencil for the stress terms uses only three nodes in each of the three directions.

With the above described time and space discretizations, Eq. (1) becomes:

$$\Delta\mathbf{Q}^{n+1} + \Delta\tau\left(\delta_\xi \mathbf{E}^{n+1} + \delta_\eta \mathbf{F}^{n,n+1} + \delta_\zeta \mathbf{G}^{n+1}\right) = \frac{\Delta\tau}{\mathrm{Re}}\left(\overline{\delta}_\xi \mathbf{R}^{n,n+1} + \overline{\delta}_\eta \mathbf{S}^{n,n+1} + \overline{\delta}_\zeta \mathbf{T}^{n,n+1}\right) \tag{2}$$

Application of Eq. (2) to the grid points leads to a system of non-linear, block penta-diagonal matrix equations for the unknown $\Delta\mathbf{Q}^{n+1} = \mathbf{Q}^{n+1} - \mathbf{Q}^n$, since the convection fluxes **E**, **F**, **G** are non-linear functions of the vector of unknown flow properties **Q**. Equation (2) is then linearized using the Jacobean matrices $\mathbf{A} = \partial\mathbf{E}/\partial\mathbf{Q}$ and $\mathbf{C} = \partial\mathbf{G}/\partial\mathbf{Q}$. This results in a system of linear, block penta-diagonal matrix equations, which is considerably expensive to solve. The approach used here is to employ an approximate factorization and the diagonal algorithm of Pulliam and Chaussee (1981), to diagonalize **A** and **C**. This approach yields:

$$\mathbf{T}_\xi^n\left[\mathbf{I} + \Delta\tau\,\delta_\xi \Lambda_\xi^n\right]\mathbf{N}^n\left[\mathbf{I} + \Delta\tau\,\delta_\zeta \Lambda_\zeta^n\right]\left(\mathbf{T}_\zeta^{-1}\right)^n \Delta\mathbf{Q}^{n+1} = \mathbf{RHS}^{n,n+1} \tag{3}$$

The solution of Eq. (3) involves two block-tridiagonal systems where the blocks are diagonal matrices.

The use of standard central differences to approximate the spatial derivatives can give rise to the growth of high frequency errors in the numerical solution with time. To control this growth, a set of 2nd/4th order non-linear, spectral radius based, explicit artificial dissipation terms are added to the discretized equations.

A slightly modified version of the Baldwin-Lomax algebraic turbulence model is used, where the maximum shear stress is used instead of the wall shear stress because in the vicinity of separation points, the shear stress values approach zero at the wall. It should be noted that this change to the Baldwin-Lomax model allows the method to treat mild separation, but it is not clear to what extent the results would be valid for massive separation. Nevertheless, considering that the model was readily available and that other turbulence models may also have difficulties with massive separation cases, the present model was applied to the problem at hand.

3. APPLICATION TO THE HEMISPHERE-CYLINDER

The numerical method described in the previous section was applied to a hemisphere-cylinder body as follows: a two-dimensional algebraic computational grid was rotated so as to generate a 3-D grid around half of the cylindrical body, so that each η-plane corresponds to a longitudinal plane. The resulting grid had 91 (longitudinal direction) $\times$ 38 (azimuthal direction) $\times$ 55 points (normal direction). The computational grid is illustrated in Figure 1.

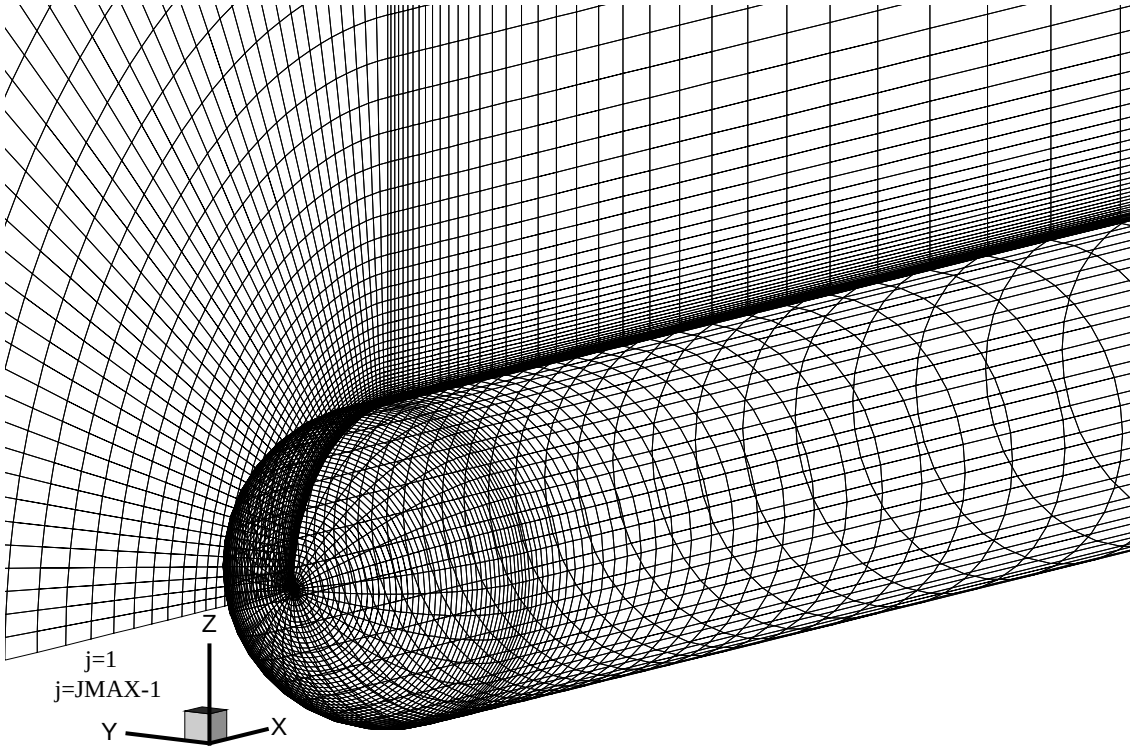

Figure 1: Computational Grid

In the longitudinal direction, half of the grid points were placed in the hemispherical section, to allow improved resolution were flow quantities are expected to vary rapidly. Aft of the hemisphere-cylinder junction, the grid was gradually spaced to cover 13 diameters in length. This length was chosen to allow simple extrapolation of flow quantities at the i=IMAX boundary. The cylinder base was not resolved (the grid i=IMAX boundary is at the cylinder base), and thus application of characteristic-based or even characteristic-compliant boundary conditions at the i=IMAX boundary would be inconsistent.

Approximately non-reflective boundary conditions (Giles, 1990) were applied at the k=KMAX boundary.

In the azimuthal (j) direction, the method solves for flow variables from the plane j=2 to j=JMAX-1. At the planes j=1 and J=JMAX, periodic boundary conditions are applied as follows: The plane j=JMAX-1 is located at the same azimuth as the plane j=1 (plane of free-stream velocity vector); the plane j=JMAX is located at the same azimuth as the plane j=2. At the end of each iteration, flow properties at j=1 are updated with flow properties at j=JMAX-1 and flow properties at j=JMAX are updated with flow properties at j=2.

Simulations were performed for Mach numbers of 0.9 and 1.2. The Reynolds numbers (based on the diameter) were 4.22×10^5 and 4.50×10^5, respectively. The angles of attack ranged from 0 to 19 degrees. These conditions were chosen to allow comparisons with the experimental results obtained by Hsieh (1975a,1975b,1977). Some of the data used were obtained from Ying (1986).

4. RESULTS AND DISCUSSION

4.1 Supersonic Case

The first test case to be discussed here is a supersonic flow condition with Mach number of 1.2 and Reynolds numbers (based on the diameter) of 4.50×10^5. Several cases of supersonic flight at various incidence were investigated by Hsieh (1975b, 1977). In addition to measuring pressure coefficients and section normal forces, Hsieh performed oil flow visualization studies which allowed the identification of the main flow features, as shown in Figure 2.

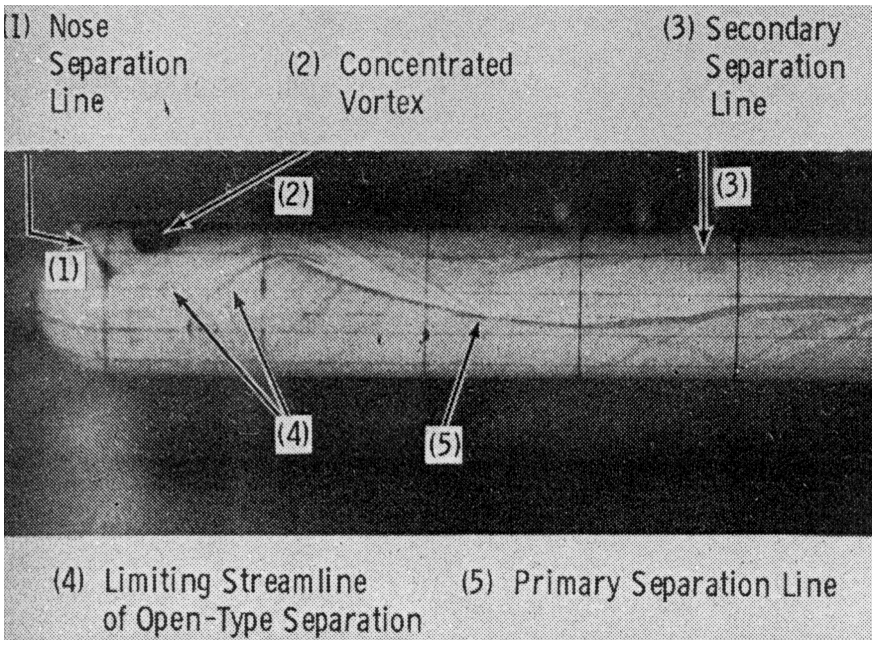

Figure 2: Typical flow features as determined from experiment (Hsieh, 1977)

Hsieh's oil flow pictures showed cross-flow separation lines starting about 1.5 diameters from the nose at angles of attack from 10°. An oblique nose separation line ahead of the hemisphere-cylinder junction and a concentrated vortex on the top of the cylindrical section are also visible at angles of attack of 15° and above (intermediate angles of attack are not available). A secondary cross-flow separation line near the top center of the cylindrical section is also visible at angles of attack of 15° and above.

The Reynolds numbers at which Hsieh's experiments were conducted are in the transition range. However, the angles of attack and Mach numbers involved are such that transition is likely to occur early in the hemispherical section. Bippes and Turk (1984) conducted oil flow visualization studies for a hemisphere cylinder at various Reynolds and (subsonic) Mach numbers, with natural and forced transition. Their low Reynolds number (3 and 6×10^5) experiments were conducted at very low Mach numbers (0.09 and 0.18, respectively). For those conditions, a short laminar separation bubble seemed to develop just forward of the hemispherical-cylinder junction. For higher Mach numbers a larger turbulent separation bubble – and open separation at higher angles – may be observed.

The numerical procedure used in the present work does not include any prediction of transition location, which may be arbitrarily set. For the conditions under consideration, the flow was considered completely turbulent.

Several cases were studied for the present investigation, but for conciseness only a couple will be shown. The first case is for a Mach number of 1.2 and angle of attack of 19°. Pressure coefficient distributions are shown in Figure 3. A good agreement with the experimental results may be observed in the wind- and leeside, as well as in the 90°-plane. This is specially encouraging because in this case, a large separated region occurs on the top of the body.

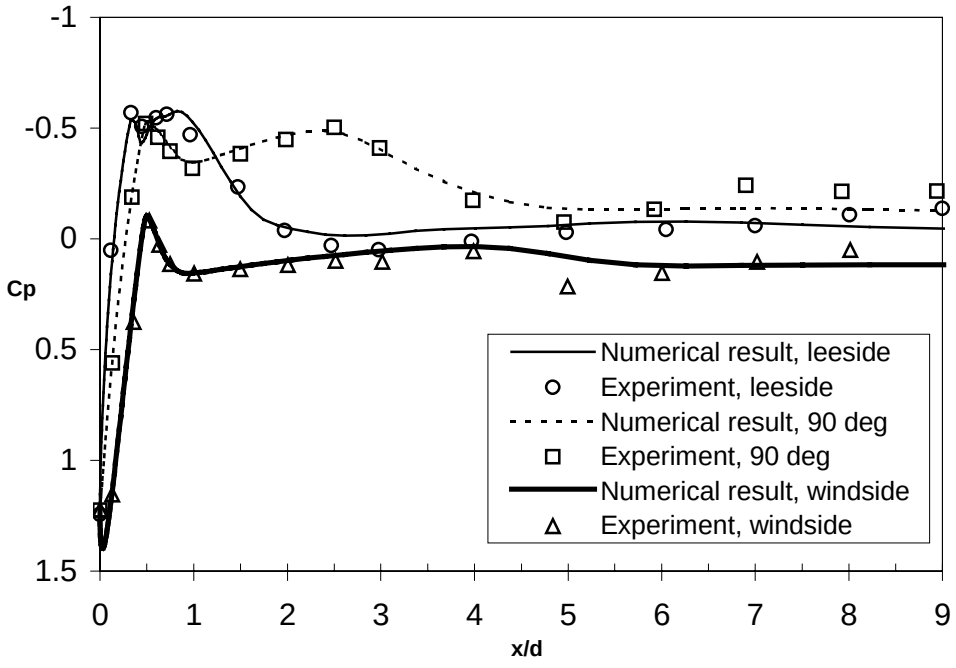

Figure 3: Pressure Coefficient Distributions, M_∞=1.2; α=19°

The main separating characteristics are well illustrated in Figure 4, where the skin friction coefficient distribution over the surface is shown. The nose separation region and cross-flow separation boundary are very clear. A region of negative skin friction coefficients, which indicates separated flow, is also apparent on the top region, aft of the hemisphere-cylinder. In this figure it may also be seen that the solution is not symmetrical. It should be noted that these results were obtained for "practical" convergence, that is for residuals decreasing 3 orders of magnitude. Although no convergence study was performed, it appears that the solutions does not converge but approaches a limit-cycle, which may be associated with alternating vortices in the top region. Therefore, Figure 4 should be considered as an "instantaneous" picture, rather than a steady-state solution.

Mach number contours in the longitudinal plane are shown in Figure 5. The shock on the top of the cylinder is shown smeared. This is due to two shortcomings of the present implementation: first, the present method is central-difference based and hence has no distinctive shock capturing capabilities; second, the grid spacing around the shock location is not so small, as grid points were more concentrated in the hemispherical section

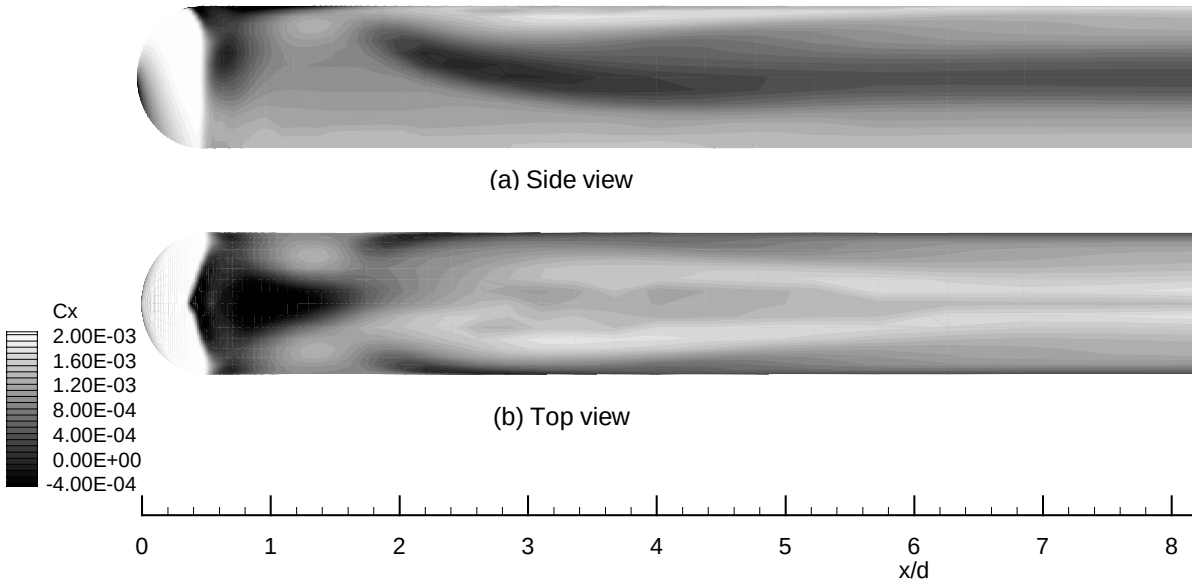

Figure 4: Skin friction coefficient contours, M_∞=1.2; α=19°

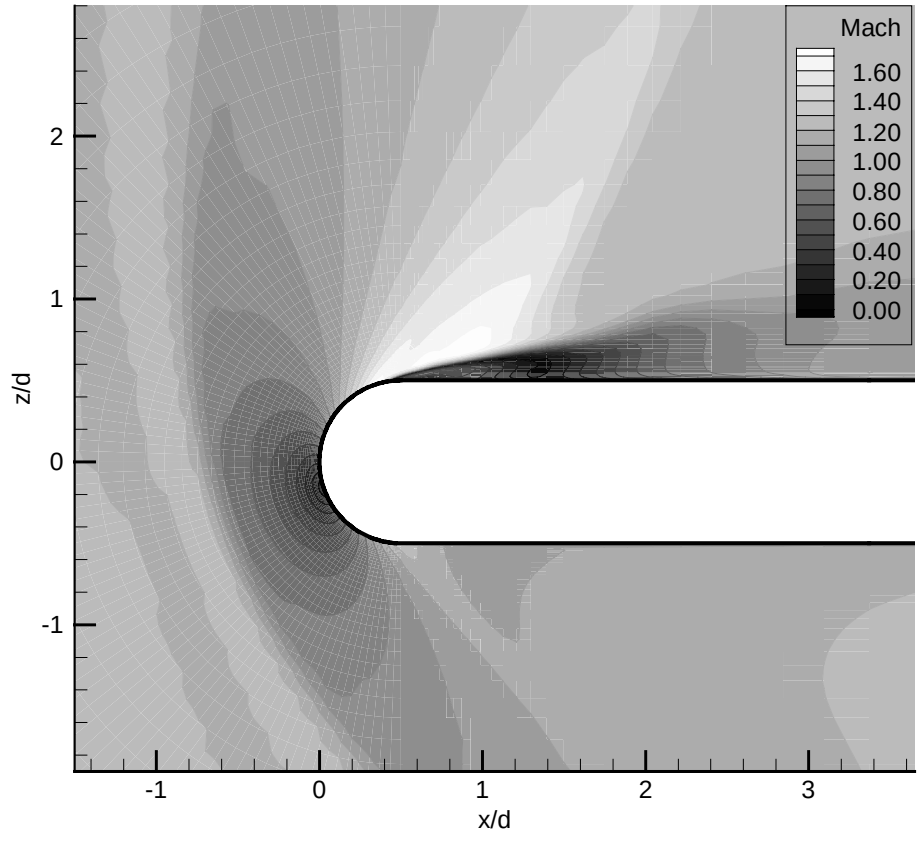

Figure 5: Mach number contours on longitudinal plane, M_∞=1.2; α=19°

The results for the main flow characteristics and local pressure distributions should allow the method to predict with a good degree of accuracy the running loads on the body. This is verified in Figure 6, where normal force coefficient distributions are compared with experimental data from Hsieh (1977) for $M_\infty = 1.2$; $\alpha = 10°$ and 19°. The numerical results compare quite well with the experiment, even around the hemisphere-cylinder junction, where sharper gradients are observed.

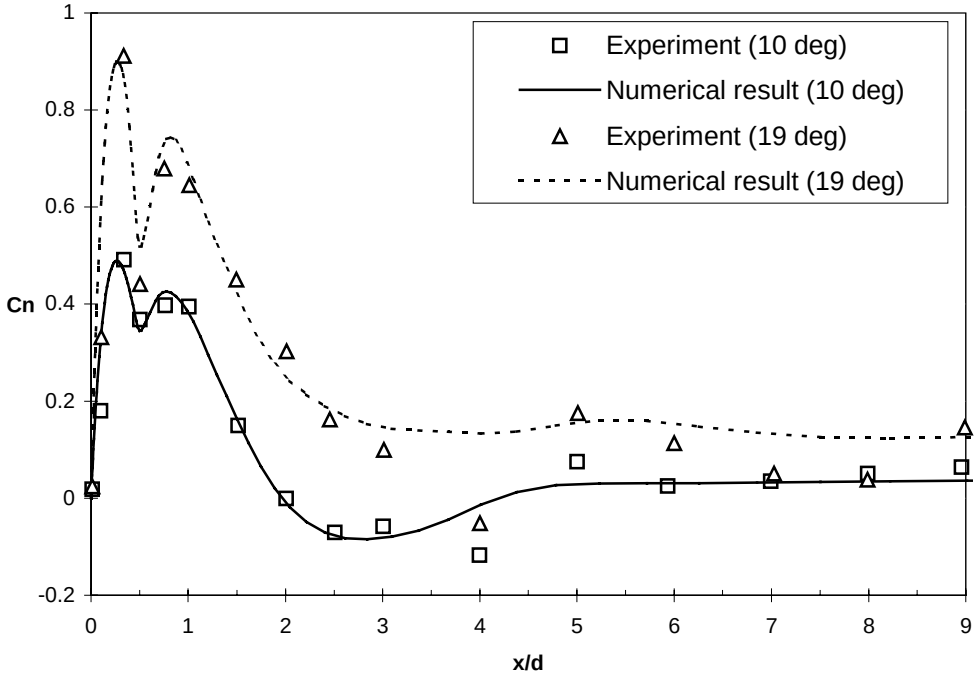

Figure 6: Normal force coefficient distribution, M_∞=1.2

4.2 Transonic Case

The next test case to be discussed here is a transonic flow condition with Mach number of 0.9 and Reynolds numbers (based on the diameter) of 4.22×10^5. The angle of attack is 19°. This is a very interesting case since the conditions resemble those encountered by the VLS first flight. Pressure coefficient distributions are shown in Figure 7. The numerical results compare fairly well with the experimental, data, except for some discrepancies on the leeside (top portion), in the separated region. The position and strength of the shock are well predicted.

Further insight into the flow in these conditions may be obtained by analyzing the skin friction contours, Figure 8. A separated region ahead of the hemisphere-cylinder junction, starting just above the windside plane is apparent, as well as a large separated region on the top region, aft of the hemisphere-cylinder junction. These areas are exactly where the discrepancies in the pressure coefficients arise. The flow is non-symmetric, and again the results should be interpreted as an "instantaneous picture" of the flow.

Additional flow details may be observed from the local Mach number contours, Figure 9. The most interesting feature here is the interaction between the shock and the separated region which seems to increase significantly downstream of the shock.

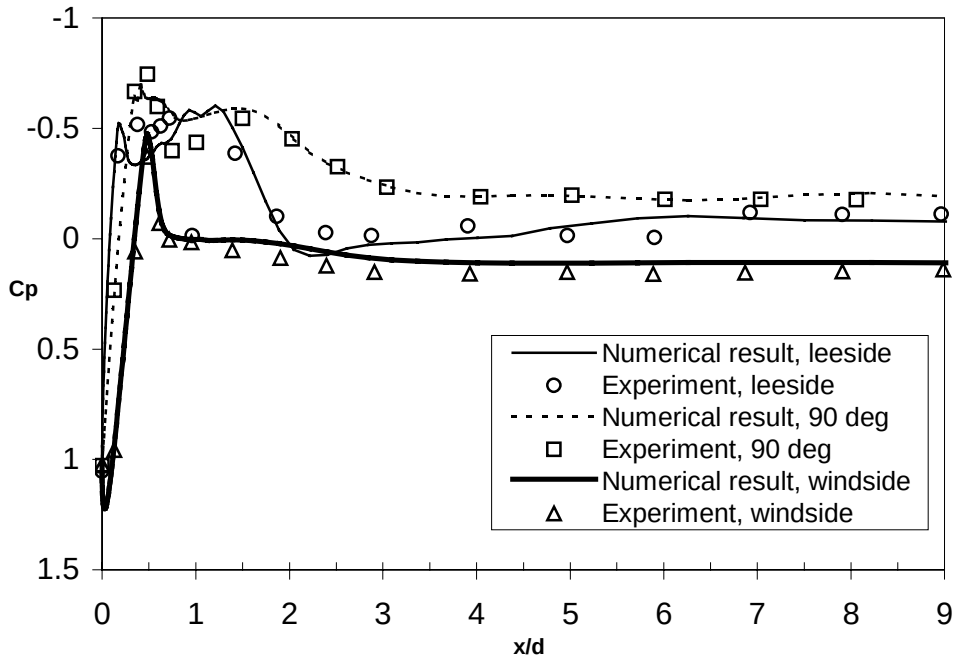

Figure 7: Pressure Coefficient Distributions, M_∞=0.9; α=19°

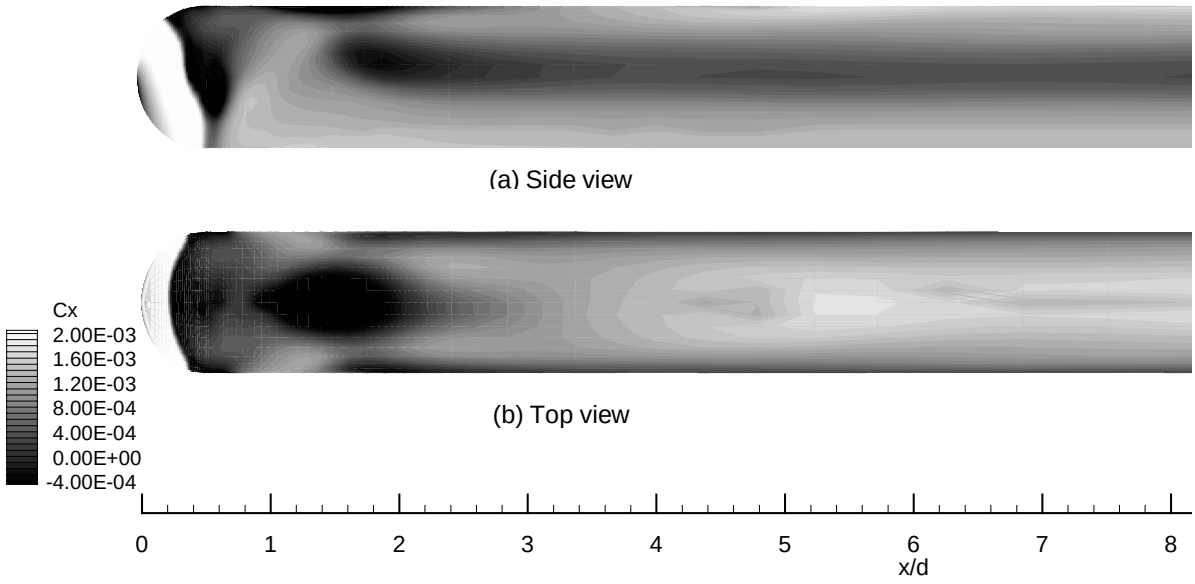

Figure 8: Skin friction coefficient contours, M_∞=0.9; α=19°

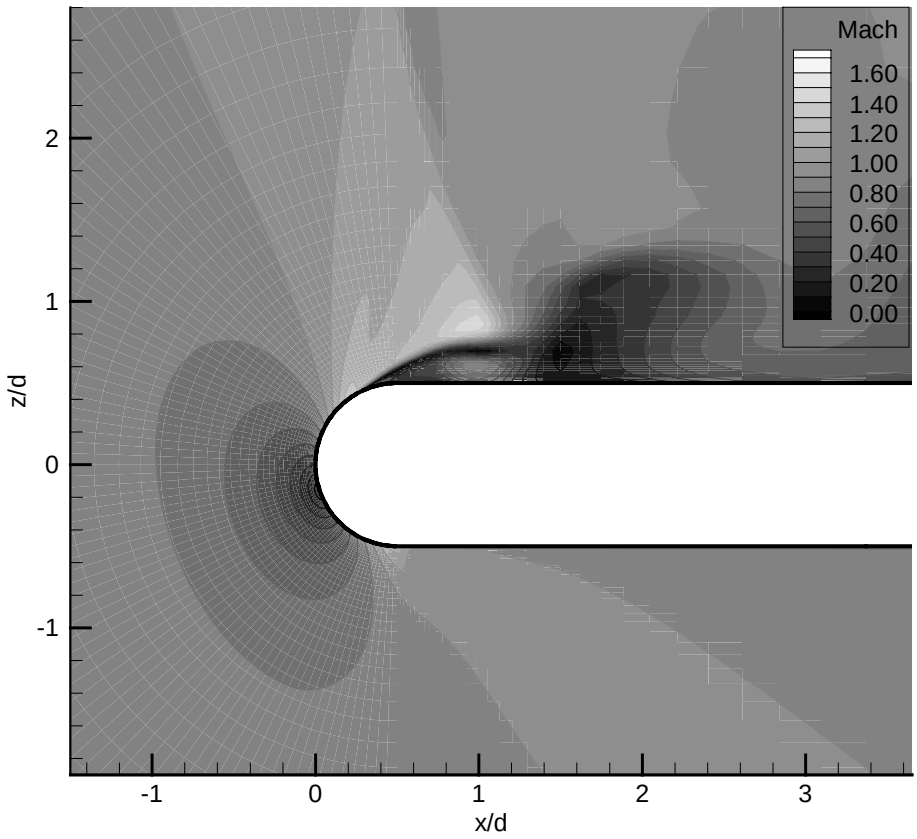

Figure 9: Mach number contours on longitudinal plane, M_∞=0.9; α=19°

5. CONCLUDING REMARKS

A Reynolds-averaged Navier-Stokes method has been applied to high angle of attack flow around a hemisphere-cylinder in supersonic and transonic flow regimes. The method used a modified Baldwin-Lomax algebraic turbulence model.

The numerical procedure was able to consistently predict the flow features as determined by published experiments. Separation patterns were quite similar to those observed in flow visualization studies.

The computed pressure coefficient and normal force distributions showed quite good agreement with experimental data, even for the highly separated flows under consideration. For the purposes of predicting the running loads on this type of configuration, the algebraic turbulent model appears to suffice.

No convergence study was performed in the present investigation, but there were indications that the solution did not converge to steady-state, but rather reached a limit cycle, which might be consistent with unsteady phenomena. Indeed, skin friction patterns showed that non-symmetric conditions are present in the solution. It is suggested that further work be pursued on the method's ability to predict the unsteady characteristics of this type of flow condition.

The present investigation corroborates previous work that showed significant non-linearity with respect to angle of attack for a rocket body configuration and indicated that the loads may not be extrapolated from lower angle results, even if this extrapolation is based on a correctly estimated total force coefficient. The present method is therefore a viable alternative for estimation of vehicle loads at high angles of attack, for which wind tunnel data may not be available.

REFERENCES

Bippes, H., & Turk, M., 1984, "Oil Flow Patterns of Separated Flow on a Hemisphere Cylinder at Incidence," Deutsche Forschungs- und Versuchsanstalt für Luft- und Raumfahrt, Institut für Experimentelle Strömungsmechanik, Göttingen, DFVLR FB 84-20.

Giles, M., 1990, "Nonreflecting Boundary Conditions for Euler Equation Calculations," *AIAA Journal*, Vol. 28, No. 12, pp. 2050–2058.

Hsieh, T., 1975, "Hemisphere-Cylinder in Transonic Flow,M_∞=0.7~1.0," *AIAA Journal*, Vol. 13, No. 10, pp. 1411-1413.

Hsieh, T., 1975, "Hemisphere-Cylinder in Low Supersonic Flow," *AIAA Journal*, Vol. 13, No. 12, pp. 1551-1552.

Hsieh, T., 1977, "Low Supersonic Flow over Hemisphere-Cylinder at Incidence," *Journal of Spacecraft and Rockets*, Vol. 14, No. 11, pp. 662-668.

Mello, O.A.F. & Azevedo, J.L.F., 1999, "Simulation of High Angle-of-Attack Flow Around the VLS Launcher Central Body," AIAA Applied Aerodynamics Conference, Norfolk, Virginia, AIAA Paper 99-3119.

Pulliam, T.H. & Chaussee, D.S., 1981, "A Diagonal Form of an Implicit Approximate-Factorization Algorithm," *Journal of Computational Physics*, Vol. 39, pp. 347–363.

Sankar, L.N. & Kwon, O.J., 1990, "High-Alpha Simulation of Fighter Aircraft," Proceedings of the NASA High Angle-of-Attack Technology Conference, Vol. 1, NASA Langley Research Center, Hampton, VA, NASA CP-3149, Pt. 2, pp. 689–702.

Ying, S. X., 1986, "Three-Dimensional Implicit Approximately Factored Schemes for the Equations of Gasdynamics," Department of Aeronautics and Astronautics, Stanford University, Stanford, CA, Rept. SUDAAR 557.